Magnetic Anisotropy of a Cyclic Octanuclear Fe(III) Cluster and Magneto-Structural Correlations in Molecular Ferric Wheels[†]

O. Waldmann,*,[‡] R. Koch,[‡] S. Schromm,[‡] J. Schülein,[‡] P. Müller,[‡] I. Bernt,[§] R. W. Saalfrank,[§] F. Hampel,[§] and E. Balthes[||]

Physikalisches Institut III, Universität Erlangen-Nürnberg, D-91058 Erlangen, Germany, Institut für Organische Chemie, Universität Erlangen-Nürnberg, D-91054 Erlangen, Germany, and Grenoble High Magnetic Field Laboratory, CNRS and MPI-FKF, 38042 Grenoble Cedex 9, France

Received November 14, 2000

The magnetic anisotropy of the cyclic octanuclear Fe(III) cluster $[Cs\subset Fe_8\{N(CH_2CH_2O)_3\}_8]Cl$ was investigated. Based on a spin Hamiltonian formalism and the consequent use of all symmetries, the magnetic anisotropy could be calculated exactly to first order, i.e., in the strong exchange limit. Experimentally, the magnetic anisotropy was investigated by magnetic susceptibility and high-field torque magnetometry of single crystals. The field and angle dependence of the torque at 1.7 K could be accurately reproduced by the calculations with one single parameter set, providing accurate results for the coupling constant and single-ion zero-field-splitting. These magnetic parameters are compared to those of several related hexanuclear ferric wheels and are discussed with respect to magneto-structural correlations for both coupling constant and single-ion anisotropy.

1. Introduction

In recent years, polyoxometalates have become the focus of intensive research activity since this class of inorganic compounds exhibits an enormous variety of structures as well as magnetic properties.[1−5] Actually, these systems often are excellent practical realizations of nanomagnets, with properties changing gradually from those of simple paramagnets to those of bulk magnets.

A particular aesthetic class is that of the ring-shaped iron(III) compounds denoted as molecular ferric wheels. The decanuclear wheel $[Fe_{10}\{(OMe)_2(O_2CCH_2Cl)\}_{10}]$ reported by Lippard et al. may be regarded as the prototype of this class.[6] Meanwhile ferric wheels with 6, 10, 12, and even 18 Fe(III) ions have been reported.[6−15] The magnetization of the ferric wheels exhibits steplike field dependencies at low temperatures due to the occurrence of field induced ground-state level-crossings—a spectacular manifestation of quantum size effects in these nanomagnets.[2] They also can be regarded as ideal model systems for the finite-size version of the linear Heisenberg chain with periodic boundary conditions. Actually, the emergence of the ferric wheels has led to a renewed interest of physicists in the properties of the Heisenberg chain, especially for large spin values.[16−18]

So far, only the Fe_6 ferric wheels have been accurately characterized for their isotropic as well as anisotropic magnetic properties.[9,11,19,20] For the Fe_{10} ferric wheel and the larger species the isotropic coupling constant could be determined, at least approximately. But the anisotropy remained largely unresolved.[6,13−15] The reason is quite obvious: The dimensions of the Hamiltonian matrixes become extremely large, being 60 466 176 for Fe_{10}. Compared to this, the calculation of the magnetic parameters for the Fe_6 wheels is actually a trivial task (the dimension is here 46 656).

Recently, we reported the new octanuclear ferric wheel $[Cs\subset Fe_8\{N(CH_2CH_2O)_3\}_8]Cl$ (**1**) (Figure 1).[12] The alkali ion is situated at the center of the octagonal wheel and stabilizes the complex. In this work we present a detailed study of the

---

* To whom correspondence should be addressed.

[†] Dedicated to Prof. Dr. Alfred X. Trautwein on the occasion of his 60th birthday

[‡] Physikalisches Institut III, Universität Erlangen-Nürnberg.

[§] Institut für Organische Chemie, Universität Erlangen-Nürnberg.

[||] Grenoble High Magnetic Field Laboratory, CNRS and MPI-FKF.

(1) Gatteschi, D.; Tsukerblat, B.; Barra, A. L.; Brunel, L. C.; Müller, A.; Döring, J. *Inorg. Chem.* **1993**, *32*, 2114.
(2) Gatteschi, D.; Caneschi, A.; Pardi, L.; Sessoli, R. *Science* **1994**, *265*, 1054.
(3) Müller, A.; Peters, F.; Pope, M. T.; Gatteschi, D. *Chem. Rev.* **1998**, *98*, 239.
(4) Gatteschi, D.; Caneschi, A.; Sessoli, R.; Cornia, A. *Chem. Soc. Rev.* **1996**, *25*, 101.
(5) Clemente-Juan, J. M.; Coronado, E. *Coord. Chem. Rev.* **1999**, *193*, 361.
(6) Taft, K. L.; Lippard, S. J. *J. Am. Chem. Soc.* **1990**, *112*, 9629.
(7) Taft, K. L.; Delfs, C. D.; Papaefthymiou, G. C.; Foner, S.; Gatteschi, D.; Lippard, S. J. *J. Am. Chem. Soc.* **1994**, *116*, 823.
(8) Caneschi, A.; Cornia, A.; Lippard, S. J. *Angew. Chem.* **1995**, *107*, 511.
(9) Caneschi, A.; Cornia, A.; Fabretti, A. C.; Foner, S.; Gatteschi, D.; Grandi, R.; Schenetti, L. *Chem. Eur. J.* **1996**, *2*, 1379.
(10) Abbati, G. L.; Cornia, A.; Fabretti, A. C.; Malavasi, W.; Schenetti, L.; Caneschi, A.; Gatteschi, D. *Inorg. Chem.* **1997**, *36*, 6443.
(11) Pilawa, B.; Desquiotz, R.; Kelemen, M. T.; Weickenmeier, M.; Geisselman, A. *J. Magn. Magn. Mater.* **1997**, *177−181*, 748.
(12) Saalfrank, R. W.; Bernt, I.; Uller, E.; Hampel, F. *Angew. Chem.* **1997**, *109*, 2596.
(13) Benelli, C.; Parsons, S.; Solan, G. A.; Winpenny, R. E. P. *Angew. Chem.* **1996**, *108*, 1967
(14) Caneschi, A.; Cornia, A.; Fabretti, A. C.; Gatteschi, D. *Angew. Chem.* **1999**, 38, 1295.
(15) Watton, S. P.; Fuhrmann, P.; Pence, L. E.; Caneshi, A.; Cornia, A.; Abbati, G. L.; Lippard, S. J. *Angew. Chem.* **1997**, *109*, 2917.
(16) Schnack. J.; Luban, M. *Phys. Rev. B* **2000**, *63*, 0144418.
(17) Chiolero. A.; Loss, D. *Phys. Rev. Lett.* **1998**, *80*, 169.
(18) Waldmann, O. Submitted.
(19) Cornia, A.; Affronte, M.; Jansen, A. G. M.; Abbati, G. L.; Gatteschi, D. *Angew. Chem.* **1999**, *111*, 2409.
(20) Waldmann, O.; Schülein, J.; Koch, R.; Müller, P.; Bernt, I.; Saalfrank, R. W.; Andres, H. P.; Güdel, H. U.; Allenspach, P. *Inorg. Chem.* **1999**, *38*, 5879.

10.1021/ic0012827 CCC: $20.00

Table 1. Crystal Data for $[Cs\subset Fe_8L_8]Cl\cdot 8C_2H_5OH$

formula	$C_{64}H_{144}ClCsFe_8N_8O_{32}$	Mr	2153.03
crystal system	tetragonal	space group	$P4/n$
crystal size [mm]	0.40 × 0.35 × 0.30	μ [mm^{-1}]	1.786
a [Å]	18.300(3)	T [K]	173(2)
b [Å]	18.300(3)	P_{calcd} [Mgm^{-3}]	1.612
c [Å]	13.242(3)	reflections collected	9108
α [deg]	90	unique reflections	5103
β [deg]	90	refl. observed [I > 2σ(I)]	3779
γ [deg]	90	final $R1$ [I > 2σ(I)]	0.0449
V [Å^3]	4434.5(12)	$wR2$ (all data)	0.1431
Z	2	largest residuals [eÅ^{-3}]	2.708/−1.022

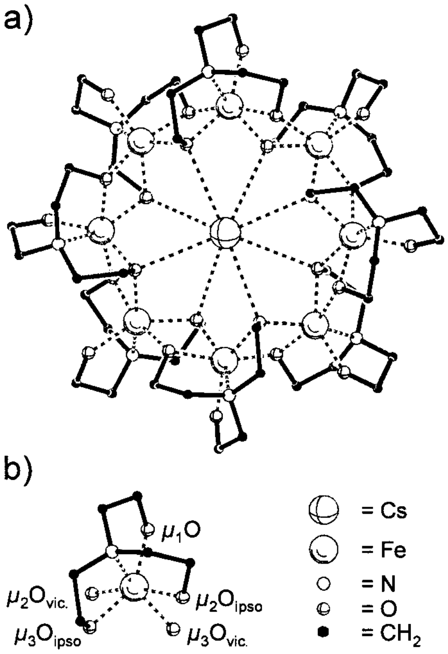

Figure 1. (a) Structure of the cation $[Cs\subset Fe_8L_8]^+$ of **2** in the crystal (PLUTON-representation; view along the crystallographic C_4 axis; H atoms omitted). (b) Detailed view of the coordination sphere of the iron center at the 12 o'clock position in (a), defining the labeling of the oxygen atoms.

magnetic properties of the Fe_8 cluster **1** by means of magnetic susceptibility and high-field torque magnetometry, with particular emphasis on the magnetic anisotropy. The Fe_8 ferric wheel is of special interest since it not only closes the gap between the Fe_6 and Fe_{10} ferric wheels but also is just at the border of what can be tackled with today's computer facilities: we will show that the calculation of the magnetic anisotropy can be achieved by the consequent use of all symmetries (the total number of states is 1 679 616). This enabled us to obtain accurate values for the coupling constant as well as the single-ion anisotropy. Finally, we compare the findings for the magnetic parameters to those of related Fe_6 ferric wheels and discuss them in the light of magneto-structural correlations.

2. Experimental Techniques

2.1. Synthesis and Characterization of the Crystal Samples. The eight membered iron-coronate $[Cs\subset Fe_8L_8]Cl$ (**1**) with L = $[N(CH_2CH_2O)_3]^{3-}$ was prepared as described in ref 12. Dissolving **1** in ethanol or acetone followed by diffusion of diethyl ether gave amber colored cuboid crystals of the solvate $[Cs\subset Fe_8L_8]Cl\cdot 8C_2H_5OH$ (**2**) or $[Cs\subset Fe_8L_8]Cl\cdot xC_3H_6O$ (**3**), respectively. For unequivocal structure characterization an X-ray structure analysis was performed on a single crystal of **2**. As will be demonstrated below, the magnetic properties of crystals of **2** and **3** are exactly the same. The presence of the unsolvated cluster **1** in **3** was confirmed by FAB spectroscopy. Compound **2** crystallizes in the space group $P4/n$. The cation $[Cs\subset Fe_8L_8]^+$ exhibits crystallographic C_{4h} molecular symmetry with the eight iron atoms forming an almost regular octagon.

X-ray structural data for $[Cs\subset Fe_8L_8]Cl\cdot 8C_2H_5OH$ was collected on a Nonius Kappa CCD area detector using Mo Kα radiation (λ = 0.71073 Å). The structure was solved by direct methods with SHELXS-97[21] and refined with full-matrix least-squares against F^2 with SHELX-97.[22] Hydrogen atoms were fixed in idealized positions using a riding model. An absorption correction was applied. Details for crystal data, data collection, and refinement are given in Table 1. Crystallographic data (excluding structure factors) for **2** were deposited with the Cambridge Crystallographic Data Centre, Deposition Number CCDC 154233. Copies of the data can be obtained free of charge on application to CCDC, 12 Union Road, Cambridge CB2 1EZ, UK (fax, (+44)1223−336−003; e-mail, deposit@ccdc.cam.ac.uk).

2.2. Magnetic Susceptibility Measurements. A single crystal was selected by light microscopy in the mother liquor. Then, the crystal was put directly from the solution into Apiezon grease and mounted on a plastic straw. The weight of the crystal samples was typically 10 μg. The magnetic moment was measured with a Quantum Design SQUID magnetometer. The temperature range was 1.8−250 K and the maximum field was 5.5 T. The susceptibility was determined from measurements at fields of 1 T. The background signal of the straw and the grease was found to be below the sensitivity of the magnetometer. Each crystal was measured repeatedly at several mutually perpendicular field directions. The molecular C_4 axis was aligned with an accuracy of ±7° parallel and perpendicular to the magnetic field. The weight of the crystals could be determined only roughly, the susceptibility data was therefore normalized as to yield g = 2.

2.3. Torque Measurements. The torque of single-crystal samples was measured with a homemade silicon-cantilever torquemeter which provides a resolution of 10^{-11} Nm (see chapter 2.4). The torquemeter was either inserted into a 15 T/17 T cryomagnet system with variable temperature insert or into the M6 magnet at the Grenoble High Magnetic Field Laboratory (GHMFL) providing up to 23.15 T. In both cases the lowest temperature was 1.7 K. The orientation of the molecular C_4 axis of the crystals with respect to the magnetic field could be aligned in situ with an accuracy of ±0.3°. As for the susceptibility measurements, a single crystal was selected by light microscopy in the mother liquor, put into grease, covered carefully with grease, mounted on the cantilever, and then cooled as quickly as possible. After a maximum of 15 min the crystal was at temperatures below 150 K. The weight of the crystal samples was typically 10 μg. The background signal of the cantilever

---

(21) Sheldrick, G. M. *SHELXS97. Program for the Solution of Crystal Structures*; University of Göttingen: Germany, 1997.

(22) Sheldrick, G. M. *SHELXL97. Program for the Refinement of Crystal Structures*; University of Göttingen: Germany, 1997

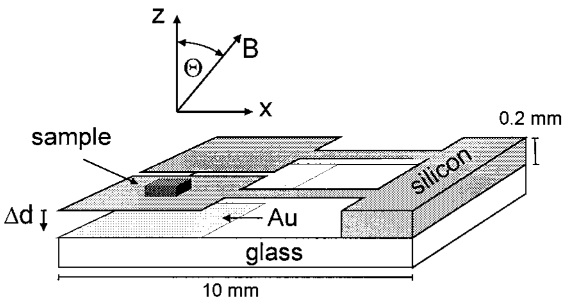

Figure 2. Sketch of the silicon double-cantilever torquemeter described in chapter 2.3.

and the grease could be neglected. A total of 10 single crystals of **2** and **3** were investigated with the 15 T/17 T setup and one single crystal of **2** with the M6 magnet. The nonlinearity $\alpha K\tau$ (chapter 2.4) was smaller than 10% for all samples.

2.4. Silicon-Cantilever Torquemeter. A schematic drawing of our cantilever torquemeter is presented in Figure 2. The main part is a double-cantilever device micromachined in one piece out of a wafer of crystalline silicon using anisotropic etching techniques. The use of crystalline silicon guarantees excellent mechanical as well as magnetic properties. The thickness of the cantilevers is about 15 μm, but that can be controlled in a wide range during the etching process. A thin gold layer is evaporated on the bottom sides of the cantilevers. The cantilever device is glued onto a glass substrate with two appropriate gold pads evaporated on it. Each cantilever together with its associated gold pad forms a capacitor.

The functional principle is simple: The torque exerted by the sample mounted on one of the cantilevers leads to a deflection of this cantilever which is detected by a change of capacity. For capacitive readout the two cantilever capacitors were connected to a ratio transformer forming an ac bridge. With this arrangement a sensitivity of $\Delta C/C_0 = 10^{-7}$ is readily obtained.[23,24] Here, C_0 denotes the zero-field capacitance (ca. 1 pF) and ΔC the change due to a deflection Δd.

The properties of the cantilever torquemeter can be modeled as follows. The torque τ leads to a deflection $\Delta d = (3/2)\tau/(DL)$ where D is the spring constant and L the length of the cantilever. Approximating the capacitors as plate capacitors, this deflection in turn results in a capacitance change of $\Delta C/C_0 \approx \Delta d/d_0(1 + \Delta d/d_0)$. d_0 is the distance of the capacitor plates. This equation shows that a cantilever torquemeter is inherently nonlinear. Finally, the capacitance bridge gives an output voltage U of $U = U_0(\Delta C/C_0)$, where U_0 is a characteristic of the bridge. Putting all together, one obtains

$$U = K\tau(1 + \alpha K\tau) \qquad (1)$$

K is the calibration constant of the torquemeter, and α is a nonlinearity parameter. In principle, these two parameters can be calculated from D, L, d_0, and C_0, i.e., from the geometry of the torquemeter, but the result might be inaccurate by a factor of 2. If K and α are required they should be obtained from an explicit calibration which can be done quite easily in many ways.[24,25]

3. Hamiltonian and Energy Spectrum

The appropriate spin Hamiltonian for a spin cluster consisting of high-spin Fe(III) ions is[9,11,19,20]

$$H = -\sum_{i<j} J_{ij}\mathbf{S}_i\cdot\mathbf{S}_j + \sum_{i<j}\mathbf{S}_i\cdot\mathbf{D}_{ij}^{dip}\cdot\mathbf{S}_j + \sum_{i}\mathbf{S}_i\cdot\mathbf{D}_{i}^{lig}\cdot\mathbf{S}_i + \mu_B\sum_{i}\mathbf{S}_i\cdot\mathbf{g}_i\cdot\mathbf{B} \qquad (2)$$

with $\mathbf{S}_i = {}^5/_2$ and the standard terms: a Heisenberg term due to exchange interactions, a dipole−dipole interaction term, a zero-field-splitting (ZFS) term due to ligand-field interactions, and the Zeeman term, respectively. An anisotropic exchange interaction term is generally neglected[9,11,19,20] since for the Fe(III) centers with their weak g-factor anisotropy it is expected to be small compared to the dipole−dipole interaction.[28] For an octanuclear cluster the dimension of the Hilbert space is as large as 1 679 616. It is thus clear that, for an accurate estimation of the magnetic properties, one has to exploit the symmetries of Hamiltonian eq 2 as far as possible, as well as to resort to suitable approximations. Hamiltonian eq 2 exhibits spin permutational (SP) symmetry[26] and for B = 0 spin flip (SF) symmetry. SP symmetry is related to the point group symmetry of the spin cluster and thus often has been denoted so but is of different significance.[26] These two symmetries alone still do not allow to solve eq 2. Recognizing that the Heisenberg exchange term additionally exhibits spin rotational (SR) symmetry, a perturbational scheme can be set up as follows.

With $J_{ij} = J + \Delta J_{ij}$ and $\mathbf{g}_i = \mathbf{g} + \Delta\mathbf{g}_i$, Hamiltonian eq 2 may be written as $H = H_0 + H_1$ such that H_0 is invariant with respect to all mentioned symmetries, SP, SF, and SR, while H_1 exhibits only SP and SF symmetry:

$$H_0 = -J\left(\sum_{i}^{7}\mathbf{S}_i\cdot\mathbf{S}_{i+1} + \mathbf{S}_8\cdot\mathbf{S}_1\right) + \mu_B\mathbf{S}\cdot\mathbf{g}\cdot\mathbf{B} \qquad (3a)$$

$$H_1 = -\sum_{i<j}\Delta J_{ij}\mathbf{S}_i\cdot\mathbf{S}_j + \sum_{i<j}\mathbf{S}_i\cdot\mathbf{D}_{ij}^{dip}\cdot\mathbf{S}_j + \sum_{i}\mathbf{S}_i\cdot\mathbf{D}_{i}^{lig}\cdot\mathbf{S}_i + \mu_B\sum_{i}\mathbf{S}_i\cdot\Delta\mathbf{g}_i\cdot\mathbf{B} \qquad (3b)$$

Here, H_0 has been already specified to a regular octanuclear spin cluster for which the spin permutations form the group D_8. The eigenstates of H_0 may be classified according to the irreducible representations (IRs) of D_8 and the spin and magnetic quantum numbers S and M, respectively. SF symmetry is of no further advantage since the SF parity is simply $(-1)^S$. Exploiting the full symmetry of H_0 all eigenvalues and eigenvectors can be calculated numerically using irreducible tensor operator and group theoretical projection techniques[27,26]

The additional energy shifts due to H_1 are now accounted for by first-order perturbation theory, i.e., J is assumed to be the dominant term. This approach is well justified for hexanuclear ferric wheels,[9,20] but its accuracy will be tested below, experimentally. The splitting of the coupling constants J_{ij} into $J + \Delta J_{ij}$ is necessary for a consistent perturbational treatment since the ΔJ_{ij} values are certainly smaller than J for the almost regular octagon $[Cs\subset Fe_8L_8]^+$. Since D_8 contains one-dimensional as well as two-dimensional IRs, many of the eigenstates of H_0 are doubly degenerate, besides the trivial degeneracy in

---

(23) Richardson, R. C.; Smith, E. N. *Experimental Techniques in Condensed Matter Physics at Low Temperatures*; Addison-Wesley Publishing Company, Inc: California, 1988.

(24) Waldmann, O.; Steinmeyer, F.; Müller, P.; Neumeier, J. J.; Régi, F. X.; Savary, H.; Schneck, J. *Phys. Rev. B.* **1996**, *53*, 11825.

(25) Schwarz, M. P.; Grundler, D.; Meinel, I.; Heyn, C.; Heitmann, D. *Appl. Phys. Lett.* **2000**, *76*, 3564.

(26) Waldmann, O. *Phys. Rev. B* **2000**, *61*, 6138.

(27) Gatteschi, D.; Pardi, L. *Gazz. Chim. It.* **1993**, *123*, 231.

(28) Bencini, A.; Gatteschi, A. *Electron Paramagnetic Resonance of Exchange Coupled Systems*; Springer-Verlag: Berlin, Germany, 1990.

M. This has to be accounted for properly by the perturbation treatment.[20] However, in the following, only nondegenerate states are of importance. For them the results of the first-order perturbation approach is equivalent to the well-known method of introducing an effective spin Hamiltonian H_n for each eigenstate of H_0:[28]

$$H_n = \Delta_n \mathbf{1} + \mathbf{S}\cdot\mathbf{D}_n\cdot\mathbf{S} + \mu_B \mathbf{S}\cdot\mathbf{g}_n\cdot\mathbf{B} \tag{4}$$

The quantities Δ_n, $\mathbf{D}_n$, and $\mathbf{g}_n$ are related to the microscopic parameters of eq 2 via $\Delta_n = -\sum_{i<j} a_{ij}^n J_{ij}$, $\mathbf{D}_n = \sum_{i<j} b_{ij}^n \mathbf{D}_{ij}^{dip} + \sum_i c_i^n \mathbf{D}_i^{lig}$, and $\mathbf{g}_n = \sum_i d_i^n \mathbf{g}_i$. Here it is worth while to note that the factors *a*, *b*, *c*, and *d* reflect the spin permutational properties of H_0 while the microscopic parameters J_{ij}, $\mathbf{D}_{ij}{}^{dip}$, $\mathbf{D}_i{}^{lig}$, and $\mathbf{g}_i$ are connected by symmetry operations of the point group of the complex. This clarifies the different significance of spin permutational and point group symmetry.

The D_8 symmetry of H_0 requires that $a_{ij} = a_{i+1,j+1}$. Assuming that only nearest-neighbor interactions are nonzero, this yields $\Delta_n = -a_n J$ with $a_n = \sum_i a_{i,i+1}^n$. Therefore, the possible alteration of the coupling strengths along the ring in $[Cs\subset Fe_8L_8]^+$ produces no effects in first order in the energy spectrum. This is equivalent to set all $\Delta J_{ij} = 0$ in H_1. The exchange interaction is then completely characterized by the single constant J.

The D_8 symmetry also implies that $c_i^n = c_{i+1}^n$ and thus $\sum_i c_i^n \mathbf{D}_i^{lig} = c_i^n \sum_i \mathbf{D}_i^{lig}$, i.e., the ligand field contribution to $\mathbf{D}_n$ is determined by an average over all $\mathbf{D}_i{}^{lig}$. Since the tensors $\mathbf{D}_i{}^{lig}$ are connected by the C_{4h} symmetry of $[Cs\subset Fe_8L_8]^+$ only components parallel to the main symmetry axis survive. $\sum_i \mathbf{D}_i^{lig}$ is thus strictly uniaxial irrespective of the actual single-ion symmetries. Then it is mathematically equivalent to replace the ligand-field term in the microscopic Hamiltonian eq 2 by $D^{lig}\sum_i[S_{i,z}^2 - 1/3\mathbf{S}_i^2]$, i.e., the ligand-field interaction is completely characterized by one single constant D^{lig}. The dipole−dipole contribution to $\mathbf{D}_n$ is also uniaxial and can be expressed as $b_n D^{dip}$ where $D^{dip} = \mu_0 \mu_B^2 g^2/(4\pi R_{i,i+1}^3)$. For the ZFS term in eq 4 one finally obtains $\mathbf{S}\cdot\mathbf{D}_n\cdot\mathbf{S} = D_n[S_z^2 - 1/3\mathbf{S}^2]$ with $D_n = b_n D^{dip} + c_n D^{liq}$.

Since also $d_i^n = d_{i+1}^n$ and moreover $d_i^n = 1/8$, $\mathbf{g}_n = \mathbf{g}$ where $\mathbf{g}$ is strictly uniaxial. This shows that the $\Delta\mathbf{g}_i$ in H_1 produce no effects in first order and may be set to zero. Additionally, the Zeeman splitting is completely characterized by two parameters $g_{||}$ and $g_\perp$. However, since $g_{||} - g_\perp$ is rather small for the Fe(III) ions, we use an isotropic g-factor as first approximation.

The splitting of the Hilbert space exploiting SR as well as the full SP, i.e., D_8, symmetry is given in Table 2. The dimension of the largest matrix is only 2085; this along with taking further advantage of the fact that the terms of H_1 commute with the spin permutations enabled us to calculate the values for a_n, b_n, and c_n with a standard personal computer. For the four lowest eigenstates these values are given in Table 3; their spectrum is drawn schematically in Figure 3. For the calculations the coupling scheme was chosen as $\mathbf{S} = \mathbf{S}_{1357} + \mathbf{S}_{2468}$, $\mathbf{S}_{1357} = \mathbf{S}_{15} + \mathbf{S}_{37}$, $\mathbf{S}_{2468} = \mathbf{S}_{26} + \mathbf{S}_{48}$, $\mathbf{S}_{15} = \mathbf{S}_1 + \mathbf{S}_5$, $\mathbf{S}_{37} = \mathbf{S}_3 + \mathbf{S}_7$, $\mathbf{S}_{26} = \mathbf{S}_2 + \mathbf{S}_6$, $\mathbf{S}_{48} = \mathbf{S}_4 + \mathbf{S}_8$.

Now the question arises of how large |D/J| can be for the first order approximation, from which eq 4 resulted, to be still justified. For the hexanuclear ring it has been explicitly tested in ref 20 that the first-order results are accurate to within 1.5% for a ratio of |D/J| as large as 0.05. At first this sounds astonishing since the splitting of the lowest S = 1 state of $D_1 = 0.68$ |J| is then already comparable to the S = 0 ↔ S = 1 level distance of $\Delta_1 = 0.69$ |J|. However, the perturbation H_1, which exhibits SP symmetry, cannot mix the S = 0 and S = 1 states since they belong to different IRs of the SP group. A view in Figure 3 reveals that the first state which mixes with the S = 0 state is the lowest S = 2 level being Δ_2 apart. The conclusion is that for the lowest levels (which are detected in most experiments) the effective spin Hamiltonian eq 4 and in particular the values presented in Table 3 are valid for a rather large ratio of |D/J|.

Table 2. Classification Scheme for a High-spin Fe(III) Octanuclear Ring Cluster in the D_8 Group

S	A_1	A_2	B_1	B_2	E_1	E_2	E_3	total
0	213	140	140	213	350	315	315	2666
1	442	503	512	433	945	980	980	7700
2	792	713	722	783	1505	1470	1470	11900
3	898	944	961	882	1845	1875	1875	14875
4	1075	996	1012	1058	2068	2038	2038	16429
5	1014	1045	1066	993	2059	2085	2085	16576
6	1013	940	961	992	1953	1927	1927	15520
7	835	854	875	814	1691	1710	1710	13600
8	736	675	696	715	1409	1390	1390	11200
9	534	544	562	516	1078	1092	1092	8680
10	422	376	394	404	798	784	784	6328
11	266	270	284	253	538	546	546	4333
12	192	161	174	178	351	343	343	2779
13	102	103	112	93	205	210	210	1660
14	68	49	58	59	117	112	112	916
15	28	28	33	23	57	59	59	462
16	19	9	14	14	27	25	25	210
17	5	5	7	3	10	11	11	84
18	4	0	2	2	4	3	3	28
19	0	0	1	0	1	1	1	7
20	1	0	0	0	0	0	0	1

Table 3. Values for the Quantities a_n, b_n, and c_n Discussed in the Text for the Lowest Spin Levels of Antiferromagnetic High-spin Fe(III) Hexanuclear and Octanuclear Rings[a]

	hexanuclear ring			octanuclear ring		
	a_n	b_n	c_n	a_n	b_n	c_n
S = 1	0.6917	20.498	−13.597	0.5366	25.033	−16.348
S = 2	2.074	5.057	−3.092	1.608	6.118	−3.808
S = 3	4.147	2.484	−1.340	3.213	2.964	−1.716

[a] The values for S = 0 are identically zero.

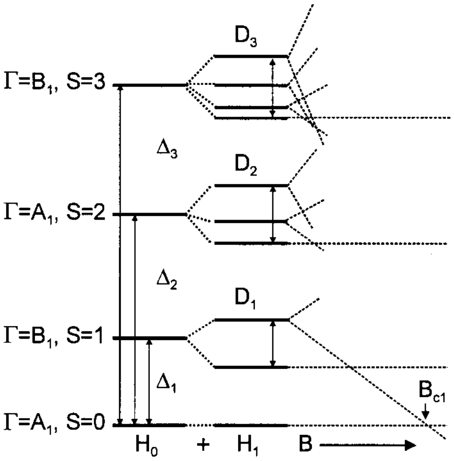

Figure 3. Schematic representation of the energy spectrum of the four lowest eigenstates of Hamiltonian eq 4. At the left, the classification of each spin level according to the IRs of D_8 and the spin quantum number S is given. B_{c1} marks the first level crossing.

4. Torque Magnetometry

For an anisotropic magnetic system the free energy is a function of the components of the magnetic field and temperature, F ≡ F(T, B_x, B_y, B_z). *x*, *y*, and *z* denote the magnetic principal axis frame. The magnetic moment vector is defined by $\mathbf{m} = -\nabla_B F$, the torque vector by $\boldsymbol{\tau} = \mathbf{m} \times \mathbf{B}$.[29] However, most magnetometers measure the projection of the magnetic moment in direction of the applied magnetic field, i.e., the measurement gives the value $\hat{m} = \mathbf{m}\cdot\mathbf{B}/B$ or $\hat{m} = -\partial F(B)/\partial B$, respectively. Analogously, a torque magnetometer measures the component of the torque with respect to a rotary axis $\mathbf{r}$. The measured value is then $\hat{\tau} = \boldsymbol{\tau}\cdot\mathbf{r}$ or $\hat{\tau} = \partial F(\varphi)/\partial\varphi$, respectively. φ is the angle of a rotation around $\mathbf{r}$. This shows that $\hat{m}$ is related to the dependence of F on the magnitude of $\mathbf{B}$, while $\hat{\tau}$ reflects the dependence of F on the orientation of $\mathbf{B}$. Interestingly, $\hat{\tau}$ can be expressed as $\hat{\tau} = \mathbf{m}\cdot(\mathbf{B} \times \mathbf{r})$. This provides an alternative viewpoint: magnetization experiments measure the component of $\mathbf{m}$ in direction of $\mathbf{B}$, torque experiments measure the component of $\mathbf{m}$ in direction of $\mathbf{B} \times \mathbf{r}$, i.e., perpendicular to $\mathbf{B}$.

Since both magnetization and torque derive from the same total differential F, both $\hat{m}$ and $\hat{\tau}$ provide the same information. But the torque technique has some experimental advantages and it is a purpose of this work to illustrate them. One point is that the torque technique allows for a rather direct access to the magnetic anisotropy since its value is closely related to anisotropy. Nevertheless it still provides the same information about the coupling constants as magnetization does. A further great advantage is that it easily allows for an in situ orientation of the magnetic field. Additionally, torquemeters are easily operated at high fields and low temperatures. (They also provide very high sensitivity, but this is not a specific advantage since nowadays magnetometers with comparable sensitivity are available.[30])

For ferric wheels it is well-known that the magnetization as well as the torque exhibit steplike field dependencies at low temperatures due to the occurrence of level-crossings:[2,19,20] Increasing the field, the ground state abruptly changes at a field B_{c1} from the zero-field $S = 0$ ground state to the first excited $S = 1$ state. At a field $B_{c2} \approx 2\ B_{c1}$ it changes to the second excited $S = 2$ state and so on (see also Figure 3). Thus it is possible to perform what may be called thermodynamic spectroscopy, i.e., the determination of the energies and splitting of individual spin levels with a thermodynamic technique.[31]

With respect to eq 4 there are two sources of information to determine Δ_n and D_n, namely the field positions of the steps or level-crossings,[19,32] respectively, and the magnitude of the torque.[20] The first approach requires the measurement of the step positions B_{cn} ($n = 1,2,...$) as function of the orientation of the magnetic field. This can be done by magnetization measurements, but torque is here greatly in favor because of its in situ orientation feature. On the basis of eq 4 the fields B_{cn} can be calculated exactly for the first step,[32]

$$B_{c1}(\Theta) = \frac{\Delta_1 + {}^1\!/_3 D_1}{g\mu_B}\left(\frac{\Delta_1 - {}^2\!/_3 D_1}{\Delta_1 + {}^1\!/_3 D_1(1 - 3\cos^2\Theta)}\right)^{1/2} \tag{5a}$$

or in the high-field limit for all steps,[19]

$$B_{cn}(\Theta) = \frac{\Delta_n + (\cos^2\Theta - {}^1\!/_3)[D_n S(S - {}^1\!/_2) - D_{n-1}(S - 1)(S - {}^3\!/_2)]}{g\mu_B} \tag{5b}$$

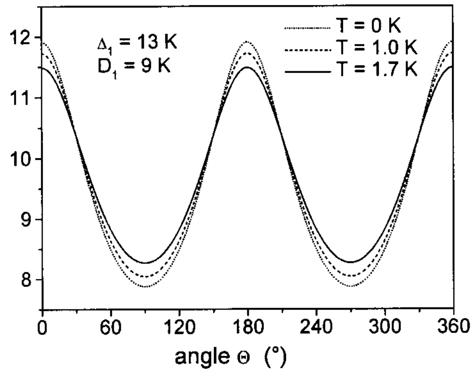

Figure 4. Calculated angle dependence of the deflection point of the first torque step due to the $S = 0 \rightarrow S = 1$ level crossing for various temperatures.

Here, Θ is the angle between magnetic field and magnetic z-axis. In these equations it has been assumed that the g-factor is isotropic, i.e., $g_\parallel = g_\perp \equiv g$.

It is important to note that, due to the high-field approximation, the range of validity of eq 5b is limited to values of $|D/J|$ smaller than about 0.003, which is much smaller than what is acceptable for eq 4. However, it is clear that for higher level-crossings, i.e., higher fields, eq 5b becomes increasingly valid.

A further point which requires consideration is how to determine the field positions of the level-crossings B_{cn} experimentally. The most sensible features of the data are the deflection points of the measured torque steps, denoted here as B^*_{cn}. It is natural to identify these deflection points with B_{cn}. However, this is only correct for very low temperatures as is shown in Figure 4. Here we have calculated $B^*_{c1}(\Theta)$ numerically for $J = -24.2$ K, $D = -0.55$ K ($\hat{=}\ \Delta_1 = 13$ K, $D_1 = 9$ K) taking into account the four lowest spin levels and the values in Table 3. Figure 4 demonstrates that already for temperatures $T \approx 0.1\ \Delta_1$ the deflection point B^*_{c1} considerably differs from B_{c1}. Since each torque step exhibits a different step height, one confirms easily that with increasing temperature the thermally broadened torque steps become less and less symmetrical; this leads to the above effect. It should be noted that a temperature of $T \approx 0.1\ \Delta_1$ is already small enough for the torque steps to be well resolved (see Figure 6). If one would analyze the $T = 1.7$ K curve in Figure 4 using eq 5a, one would obtain $\Delta_1 = 13$ K and $D_1 = 7.5$ K, i.e., D_1 would be wrong by 17%.

According to the above, eq 5 should be applied with care, but trouble can be avoided by calculating $B^*_{cn}(\Theta)$ numerically what is easily done. In any case, the approach to measure $B^*_{cn}(\Theta)$ [or $B_{cn}(\Theta)$] is an excellent tool to determine the Δ_n and D_n—as long as one relies on the validity of the spin Hamiltonian eq 4. There is little if any chance to check whether eq 4 is really valid or whether it should be better supplemented by further terms, like g-factor anisotropy, fourth order terms, etc. $B^*_{cn}(\Theta)$ does not contain enough information to do that unambiguously.

As an alternative approach, the D_n can be determined from the magnitude of the torque since it is directly related to the magnetic anisotropy:[20]

$$\hat{\tau} = m_z B_x - m_x B_z \tag{6}$$

Here, the magnetic field is applied in the xz-plane and the torque

---

[29] Jackson, J. D. *Classical Electrodynamics*; John Wiley & Sons: New York, 1975.

[30] Wernsdorfer, W.; Bonet Orozco, E.; Hasselbacj, K.; Benoit, A.; Barbara, B.; Demoncy, N.; Loiseau, A.; Pascard, H.; Mailly, D. *Phys. Rev. Lett.* **1997**, *78*, 1791.

[31] Waldmann, O.; Koch, R.; Schromm, S.; Müller, P.; Zhao, L.; Thompson, L. K. *Chem. Phys. Lett.* **2000**, *73*, 332.

[32] Cornia, A.; Jansen, A. G. M.; Affronte, M. *Phys. Rev. B* **1999**, *60*, 12177.

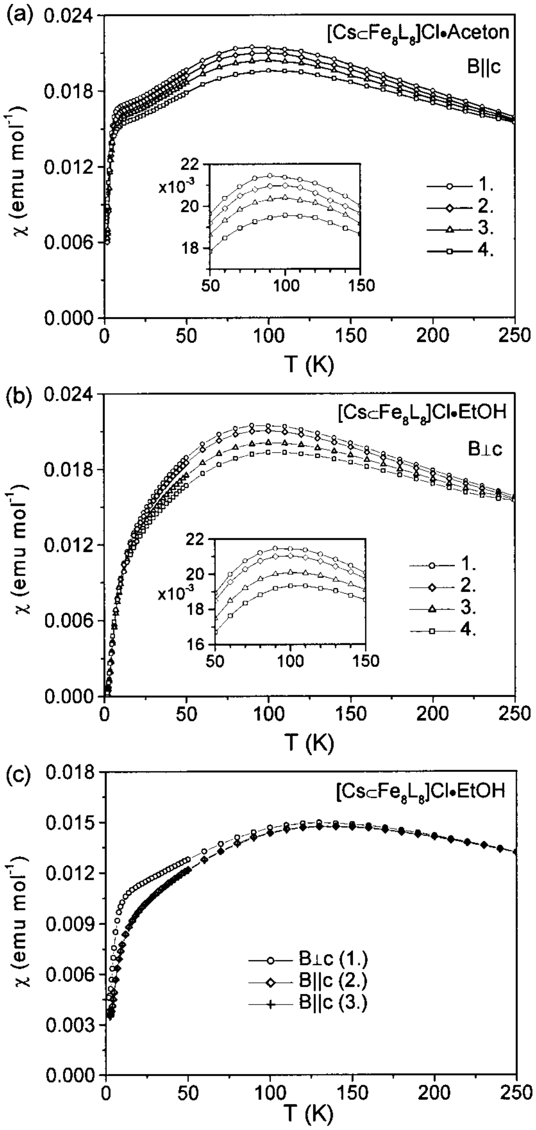

Figure 5. (a) and (b) show the temperature dependence of the magnetic susceptibility of **3** and **2**, respectively, for the first four successive temperature sweeps. The insets provide a detailed view on the temperature range 50−150 K. (c) Temperature dependence of the magnetic susceptibility for a "relaxed" crystal sample of **2** for three mutually perpendicular field directions.

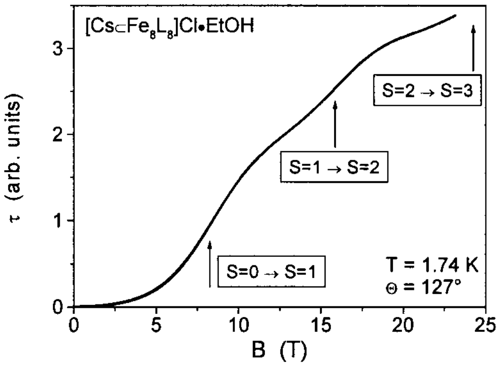

Figure 6. Typical field dependence of the torque for a crystal sample of **2**. The data shown here was measured in the M6 magnet at the GHFML.

is measured with respect to the *y*-axis. The Δ_n are still determined by the step positions.

Reversely, the accuracy of the values for D_n is directly determined by the accuracy of the calibration of the torque signal and, if one uses a cantilever torquemeter, might be further corrupted by a too large nonlinearity. Nonlinearity, however, can be avoided in most cases by selecting crystals of proper size. The calibration consists of two factors, the calibration constant of the torquemeter K and the number N of molecules of the individual crystal. With some care, K can be determined within 1−2%. Thus, the most crucial point is the determination of N. If the crystal is stable in air, this may be done by weighting.[31] If the crystal should be covered by, e.g., grease in order to prevent decomposition, one can measure the susceptibility and scale it to the data obtained for a polycrystalline sample.[20] However, to be fair, it is difficult to arrive at an (overall) accuracy better than 5%. Also, it may happen that there is no way at all to determine N—as in the present case of $[Cs\subset Fe_8L_8]^+$, see the next section.

In this work we consider angle/field dependence and magnitude of the torque simultaneously. We will then show that the data contains enough information to determine Δ_n, D_n, N, nonlinearity, etc., as well as to check the completeness of the theoretical model without the need for a calibration.

5. Magnetic Susceptibility Measurements

The magnetic susceptibility of single crystals of **2** and **3** is shown in Figure 5. Figure 5a and 5b present data for the first four successive temperature sweeps after having extracted samples of **3** and **2**, respectively, from the mother liquor. Data were collected for decreasing temperature. Obviously, the magnetic properties for both materials changed during measurement. In particular, the temperature of the maximum of χ increased starting from about 90 K (insets of Figure 5a and 5b). However, after a certain time, the samples relaxed into a final state, and reproducible measurements could be performed. This is demonstrated in Figure 5c. Here a crystal of **2** was measured for three orientations of the magnetic field. For relaxed samples the maximum of χ occurs at about 130 K. The temperature dependencies of χ in Figure 5c exhibit the behavior expected for an octanuclear ring with antiferromagnetic coupling and a hard axis anisotropy. Since the maximum temperature is directly proportional to the coupling strength, Figure 5 indicates an increase of the coupling constant by at least 40%. In the relaxed state, $J \approx -60$ K.

For the hexanuclear rings $[Li\subset Fe_6L_6]^+$ and $[Na\subset Fe_6L_6]^+$ it has been found that the coupling constant of powder samples is about 10% larger than that of crystal samples.[20] This has been attributed to structural changes due to a loss of solvent molecules in the powder samples. Obviously, in the octanuclear ring $[Cs\subset Fe_8L_8]^+$ structural changes are much more rapid and pronounced. However, it is unlikely that a loss of solvent molecules is responsible for them. First, in the case of $[Li\subset Fe_6L_6]^+$ and $[Na\subset Fe_6L_6]^+$ a loss of solvent molecules leads to a decomposition of the crystals. And second, the grease covering the crystals usually operates as a protective shield effectively preventing losses of solvent molecules. The actual mechanism is quite unclear so far and will not be discussed further.

These results show that the determination of the magnetic properties on samples of **2** (and **3**) with structures which correspond exactly to that determined by X-ray crystallography represents a problem for many experimental techniques. The technique must allow to determine the isotropic (Δ_n) and anisotropic parameters (D_n) of single crystals without ever exposing the crystals to temperatures above, e.g., 100 K. This excludes most techniques such as magnetic susceptibility measurements (clear from Figure 5), high-resolution magnetiza-

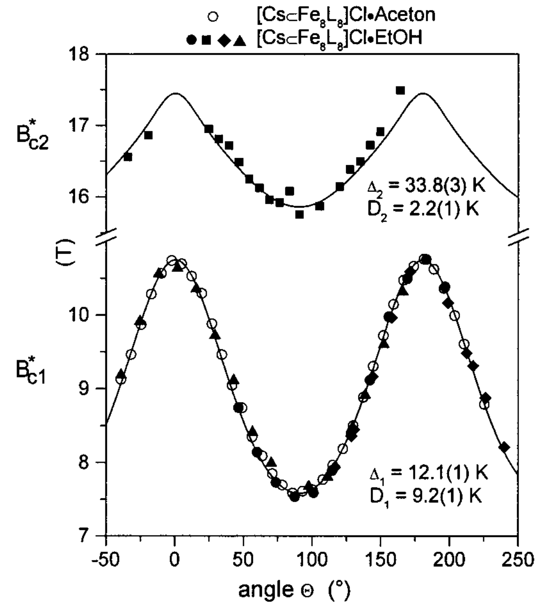

Figure 7. Angle dependence of the deflection points of the first and second torque step for various crystals of **2** and **3**. The deflection points were determined by numerical differentiation of field versus torque measurements for fixed angles at 1.7 K. The solid curves correspond to the fitting results.

tion measurements (no in situ orientation of the crystal), specific heat techniques (too low sensitivity), and inelastic neutron scattering (huge amounts of material ⟹ powder samples). Furthermore, X-band EPR-spectroscopy on single crystals of **3** gave no signal. In view of the expected broad lines the crystals were probably too small, but high-frequency EPR might be successful.

However, torque magnetometry allows for the determination of the isotropic and anisotropic parameters from measurements at low temperature without the need to warm the crystal once installed. Thus it meets all requirements to determine the "intrinsic" magnetic parameters of **2** and **3** without running into the "relaxation" problem, as will be demonstrated in the next section.

6. Torque Measurements: Results and Analysis

Figure 6 presents the typical result of a torque measurement. The positive value of the torque at an angle of $\Theta = 127°$ demonstrates a hard axis anisotropy of $[Cs\subset Fe_8L_8]^+$. This already fixes the signs of the values D_n to be positive. For fields up to 23.15 T, two torque steps due to the $S = 0 \rightarrow S = 1$ and $S = 1 \rightarrow S = 2$ level crossings can be clearly seen, the onset of a third torque step due to the $S = 2 \rightarrow S = 3$ level crossing is in the offing.

We determined the deflection points B^*_{c1} of the first torque step by numerical differentiation of the data. The resulting angle dependencies are shown in Figure 7 for several samples. Two conclusions can be drawn. First, the magnetic properties of $[Cs\subset Fe_8L_8]^+$ obviously are not influenced by the type of solvent molecules in the crystal, i.e., they are equal for **2** and **3**. Second, measurements for different samples led to equal results. This demonstrates that we indeed measured the intrinsic magnetic properties of $[Cs\subset Fe_8L_8]^+$ in its X-ray structure, unaffected by the "relaxation" effect described in chapter 5 which prevented reliable magnetization measurements. In the following we no longer discriminate between different samples, i.e., all conclusions should be understood to be valid for all samples investigated.

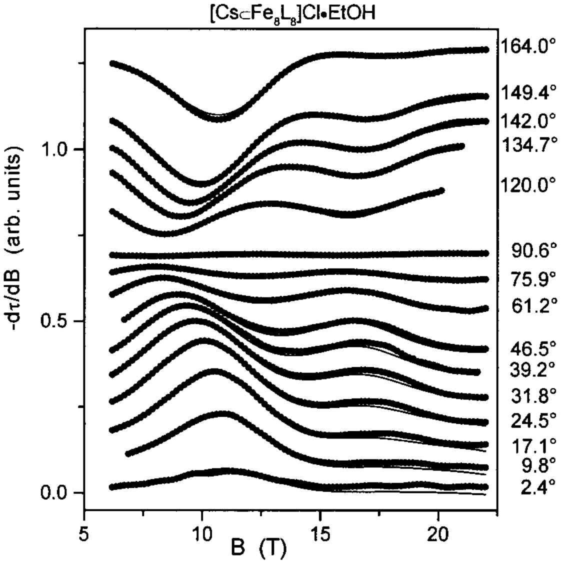

Figure 8. Field dependence of the torque, drawn as $-d\tau/dB$, for various angles and T = 1.74 K. The derivative with respect to the field was calculated numerically. The solid curves represent a typical fitting result.

The values of Δ_1 and D_1 were determined by fitting the experimental deflection points B^*_{c1} to a numerical calculation as described in chapter 4 (Figure 7). The result for Δ_1 and D_1 is given in eq 7. The agreement of theory and experiment is excellent. A similar procedure was applied for the second torque step yielding the Δ_2 and D_2 given in eq 7. Although the data for the second torque step scatters considerably more, the agreement between theory and experiment is still good.

$$\Delta_1 = 12.1(1)\ \mathrm{K},\ D_1 = 9.2(1)\ \mathrm{K}$$
$$\Delta_2 = 33.8(3)\ \mathrm{K},\ D_2 = 2.2(1)\ \mathrm{K} \qquad (7)$$

To gain more insight, we took into account the additional information contained in the magnitude of the torque signal by fitting the field-sweep data at 1.7 K for about 20 angles simultaneously with one spin Hamiltonian. Actually, for fitting, the derivative $d\tau/dB$ has been used. The data set for one crystal typically consists of a total of 2500 data points. Figure 8 presents the data set for the crystal of **2** measured in the M6 magnet at GHFML. For clarity, not all of the 24 angles are shown.

We considered the following parameters which can be divided into three groups. The first group includes the number of molecules N which could not be determined independently due to the "relaxation" effect (chapter 5), as well as the nonlinearity parameter α. The second group consists of the parameters of the effective spin Hamiltonian eq 4, namely, Δ_1, ..., Δ_3 and D_1, ..., D_3. The last group embraces parameters with a comparatively weak effect. This includes a g-factor with $g \neq 2$ and a g-factor anisotropy $\Delta g = g_{\|} - g_{\perp}$. Furthermore, in second order the Hamiltonian eq 4 has to be extended by a forth order term, $B_0^4\, O_0^4(\mathbf{S})$, and a TIP term, $-{}^1/_2\mathbf{B}\cdot\chi_0\cdot\mathbf{B}$.[33,31] The latter is parametrized by $\Delta\chi_0 = \chi_{0,\|} - \chi_{0,\perp}$.

We tried to get an impression about the importance of a particular parameter by looking at how its value depended on which parameters were included in the fit. For example, if the best fit value for Δg widely scatters depending on whether B_0^4, $\Delta\chi_0$, etc. are set as free parameters or not, we would regard Δg as being not significant. If the value of a particular parameter

---

(33) Abragam, A.; Bleaney, B. *Electron Paramagnetic Resonance of Transition Ions*; Clarendon Press: Oxford, U. K., 1970.

stayed within about 5% independent of the choice of the other parameters, we called it "stable". For each of the chosen combination of fitting parameters, we checked for a possible over-parametrization by repeating the fit for many different starting values. If over-parametrized, the fitting routine would converge to distinct sets of best fit parameters. However, in no case over-parametrization was detected. Finally we compared the values obtained for different crystals providing a further test for "stability".

The number of molecules N was always found to be a stable parameter. The values had the correct order of magnitude. Also, for those measurements with an appreciable nonlinearity (i.e., where $\alpha K\tau > 1\%$), the parameter α was stable and in good agreement with that determined independently. This demonstrates that the data indeed contains enough information to determine not only the physically interesting parameters but also N and α.

Concerning the parameters Δ_1, ..., Δ_3 and D_1, ..., D_3, it is clear that the 17 T data sets gave stable values for Δ_1 and D_1 (since they exhibit $n = 1$ torque steps) and that the 23 T data set additionally gave stable values for Δ_2 and D_2. Since for these magnetic fields the respective next higher torque steps are already in the offing, they had to be accounted for in the fit. But clearly the data do not allow the determination of both Δ_{m+1} and D_{m+1} independently (m = 1 for the 17 T and m = 2 for the 23 T data sets). Therefore, we first set D_{m+1} as free parameter and fixed Δ_{m+1} to $a_{m+1}/a_1\ \Delta_1$. The fits resulted in stable but much too large, i.e., unphysical, values for D_{m+1}. Choosing Δ_{m+1} as a free parameter with $D_{m+1} = c_{m+1}/c_1\ D_1$ also resulted in stable values for Δ_{m+1}. Since Δ_2 obtained in this way for the 17 T curves agreed well with the value from the 23 T fits, we regard the 23 T value for Δ_3 as an approximate estimate of Δ_3. Taking into account the parameters of the first and second group, the agreement factor $R[(dm/d\tau)^2]$ was always less than 2%. In view of the large data sets, this is a satisfying value.

Concerning the parameters of the third group, their inclusion led only to a slight improvement: The agreement factor R could be improved at best by a factor of 2. Furthermore, the values significantly scattered for the varying fit conditions, i.e., these parameters were not stable in the above sense. But reducing the g-factor to about g = 1.95 seemed to give consistently smaller R values. Concerning the second-order parameters, we conclude that they are too small to be determined from our experiments.

We summarize our findings as follows:

$$\Delta_1 = 12.1(3)\ \text{K},\ D_1 = 9.0(4)\ \text{K}$$
$$\Delta_2 = 33.7(6)\ \text{K},\ D_2 = 2.2(2)\ \text{K}$$
$$\Delta_3 = 70(6)\ \text{K}$$
$$g = 1.95(3) \qquad (8)$$

The esds given here reflect the statistical error, the dependence of the values on the combination of fit parameters, as well as the variation for different crystals. The values are consistent with those determined from $B^*_{cn}(\theta)$, eq 7. However, we regard eq 8 as our final result since our fitting strategy guarantees that these values are model independent within the given esds (eq 7 was obtained from an analysis where second-order contributions were neglected from the outset).

7. Discussion

The analysis in chapter 6 gave no evidence for the importance of second-order contributions to the effective spin Hamiltonian eq 4. Thus, the first-order calculation of the energy spectrum should allow for an accurate determination of the magnetic parameters J and D of the microscopic Hamiltonian eq 2 using the experimental values for Δ_n and D_n of the effective Hamiltonian eq 4.

The contribution of the dipole−dipole interaction to the ZFS of the S = 1 spin level is calculated as $D_1^{dip} = 1.98$ K ($D^{dip} = 0.0791$ K). This yields a value of $D_1^{lig} = 7.0(4)$ K, or $D^{lig} = -0.43(2)$ K for the microscopic ZFS, respectively. The value estimated from D_2 is $D^{lig} = -0.45(5)$ K which is somewhat larger than the S = 1 estimate but agrees within the error estimates, i.e., D_1 and D_2 are consistent within the framework of a first-order calculation.

In contrast, the values for J estimated from Δ_1 and Δ_2 are J = −22.5(6) K and J = −21.0(4) K, respectively. The discrepancy is significantly larger than experimental errors. However, the analysis in chapter 6 and the consistency of D_1 and D_2 implies that the values of Table 3 are correct. One might assume that the magnetic coupling paths in the $[Cs\subset Fe_8L_8]^+$ cluster are better described by two coupling constants J_1 and J_2. This is not only suggested by the C_{4h} molecular symmetry but is also consistent with the above findings: Setting $J_1 \neq J_2$ leads to a second order correction to the Δ_n but only to a third order correction to the D_n and moreover produces no second-order terms in the effective spin Hamiltonian eq 4. Increasing $|J_1 - J_2|$ has different effects than increasing the ratio $|D^{lig}/J|$. However, to explain the observed discrepancy of the J values one would require a rather large difference of J_1 and J_2, which seems unlikely in view of the crystal structure of $[Cs\subset Fe_8L_8]^+$. To find a final answer, more accurate measurements of D_n, and/or measurements of Δ_n and D_n for n > 2 would be required. To close we summarize our results as

$$J = -22(1)\ \text{K},\ D^{lig} = -0.44(3)\ \text{K} \qquad (9)$$

It is interesting to compare the values of Table 3 for the hexanuclear and the octanuclear ring. The splitting of the spin levels $\Delta_n = a_n\,|J|$ exhibits the behavior which meanwhile is widely accepted:[4] The a_n follow the Landé-rule $a_n \approx a_1\ 1/2\ n(n+1)$, whereby $a_1 \approx 4/N$. N is the nuclearity of the ring. These findings are based on a simple two-sublattice model.[4] Within the same model it is straightforward to calculate also approximations for b_n and c_n.[9] For the hexanuclear ring this model leads to values accurate to within 8%,[20] but with increasing N the accuracy decreases. A further point is of interest. According to Table 3, Δ_n increases while D_n decreases with N (with J, D^{dip}, and D^{lig} being constant). Since $|D_1/\Delta_1|$ is a measure for the importance of higher order terms in the effective Hamiltonian eq 4, we expect the strengths of higher order terms to increase with the nuclearity of the cluster.

Given the current interest in single molecule magnets (SMMs), it is of great importance to understand the factors which control the coupling strength and in particular the ZFS in order to find strategies to produce SMMs with high blocking temperatures.[34] In practice, it may be a challenging task to calculate the dipole−dipole contribution to the ZFS since precise wave functions are required. But in principle it can be done rigorously. Therefore, in the following we focus on J and D^{lig}.

Meanwhile, accurate measurements of both the coupling strength as well as the single-ion ZFS have been reported for five hexanuclear ferric wheels.[9,11,19,20] For these hexanuclear clusters and the octanuclear cluster discussed in this work, the values of J, D^{lig}, and some structural parameters are compiled

---

(34) Gatteschi, D.; Sessoli, R.; Cornia, A. *Chem. Commun.* **2000**, 725.

Table 4. Structural Parameters Discussed in the Text and Experimental Results for the Magnetic Parameters for Several Molecular Ferric Wheels[a]

cluster	α_1 [deg]	α_2 [deg]	φ [deg]	Δ_1 [K]	J [K]	D_1 [K]	D_1^{dip} [K]	D_1^{lig} [K]	D^{lig} [K]
$[Li\subset Fe_6L_6]^{+b}$	101.1	105.9	127.4	12.5	−18.1	3.9	1.60	2.3	−0.17
$[Na\subset Fe_6L_6]^{+b}$	103.3	106.4	119.0	15.9	−23.0	6.1	1.54	4.6	−0.34
$[Fe_6L_6]^c$	105.3	106.2	97.8	21.8	−31.5	11.8	1.56	10.2	−0.75
$[Cs\subset Fe_8L_8]^{+d}$	102.8	103.4	115.4	12.1	−22.5	9.0	1.98	7.0	−0.43
	102.3	104.6	112.7						
$[Li\subset Fe_6L'_6]^{+e}$	101.3	103.8		13.8	−20.0	1.67	1.78	−0.11	0.01
$[Na\subset Fe_6L''_6]^{+e}$	104.6	106.5		19.8	−28.6	6.22	1.65	4.57	−0.34

[a] The hexanuclear ferric wheels all exhibit molecular S_6 symmetry. Due to the C_{4h} molecular symmetry of $[Cs\subset Fe_8L_8]^+$ two values appear for each structural parameter (the means were used for Figures 9 and 10). L ≙ $N(CH_2CH_2O)_3$, L′ ≙ $(OMe)_2$dbm, L″ ≙ $(OMe)_2$pmdbm. [b] Refs 12, 20. [c] Refs 11, 35. [d] Ref 12 and this work. [e] Refs 9, 10, 19.

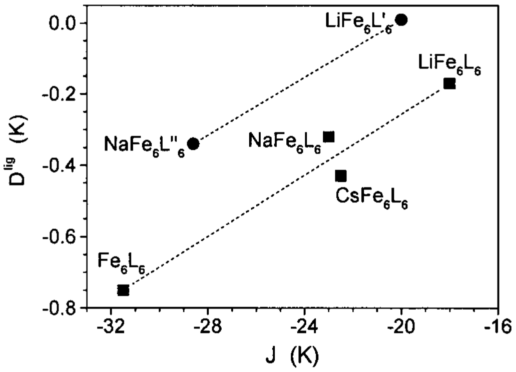

Figure 9. Single-ion anisotropy D^{lig} versus coupling strength J for the ferric wheels listed in Table 4. Dashed lines are guides to the eyes.

in Table 4. It is clear from the limited amount of experimental data available so far that it is difficult to establish any correlation conclusively. But overall trends may be visible.

Before entering a discussion of magneto-structural correlations, it is useful to consider the plot D^{lig} versus J shown in Figure 9. The data points scatter widely indicating that the two sets of structural parameters which determine J and D^{lig}, respectively, cannot be identical. This could have been anticipated from the outset since J is determined by the coupling path while D^{lig} is determined by the coordination sphere. Nevertheless, there is a clear trend for D^{lig} to increase with J, in particular if one distinguishes between the four clusters based on the triethanolamine ligand (called L-clusters) and the two clusters $[Li\subset Fe_6L'_6]^+$ and $[Na\subset Fe_6L''_6]^+$ based on β-diketonato ligands (L*-clusters), see Figure 9.

Actually, the difference of these two cluster families is evident from the different coordination spheres of the iron centers: For L-clusters it consists of one amino-nitrogen and five alkoholato oxygens (see Figure 1b), while for L*-clusters it is comprised of four alkoxy oxygens and two oxygens from the β-diketonato ligand. This difference should clearly affect the ZFS, and it is thus not reasonable to search for a common correlation of D^{lig} and structure. We regard the two clusters $[Li\subset Fe_6L'_6]^+$ and $[Na\subset Fe_6L''_6]^+$ as members of one family since the ligands L′ and L″ are quite similar, at least with respect to the first coordination sphere. That the differences of L′ and L″ are of little importance magnetically is also suggested by the insensitivity of the coupling constant, which is J = −28.6 K for $[Na\subset Fe_6L''_6]ClO_4$,[36] J = −28.8 K for $[Na\subset Fe_6L'_6]ClO_4$,[36] and J = −29.4 K for $[Na\subset Fe_6L'_6]Cl$.[8]

For weakly coupled di(alkoxo)-bridged Fe(III) complexes Le Gall et al.[37] reported a linear correlation between coupling constant and average Fe−O−Fe angle α: J[K] = −2.13 α[°] + 194. A view in Table 4 reveals that for the cyclic clusters J is neither correlated to the average Fe−O−Fe angle α nor to the larger Fe−O−Fe angle α_2 (the di-alkoxo bridge exhibits two different bridging angles, $\alpha_2 > \alpha_1$, see inset of Figure 10a). But a plot of J versus the smaller Fe−O−Fe angle α_1 reveals a linear correlation (Figure 10a). The best-fit straight line is

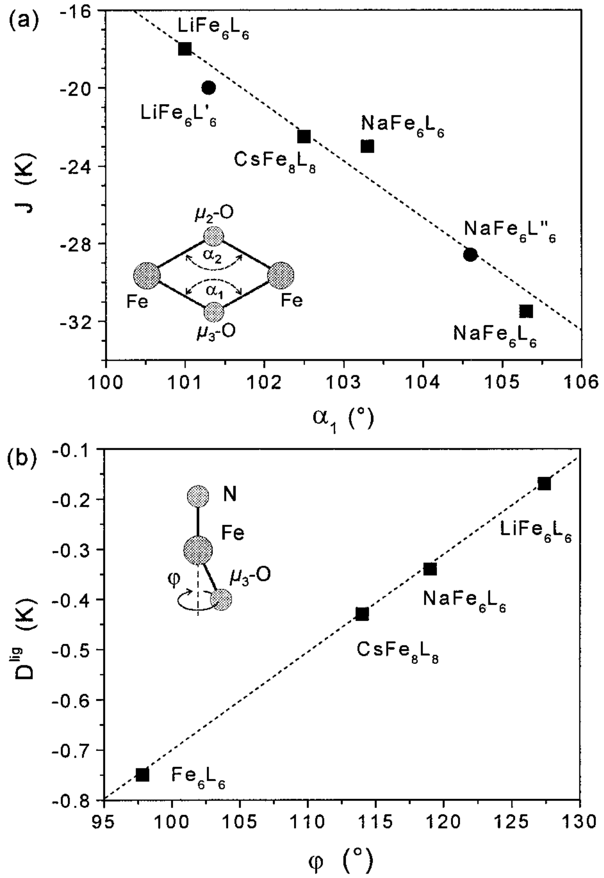

Figure 10. (a) Coupling strength J versus the smaller Fe−O−Fe angle α_1 for the ferric wheels listed in Table 4. The dashed line corresponds to the best fit line, eq 10. (b) Single-ion anisotropy D^{lig} versus rotation angle φ discussed in the text. The dashed line corresponds to the best fit line, eq 11.

$$J[K] = -2.91\,\alpha_1[°] + 276 \qquad (10)$$

As a simple model one may assume that the coupling strength is the sum of that of each coupling path, $J = J_{\alpha1} + J_{\alpha2}$. Then eq 10 expresses that $J_{\alpha2}$ either remains constant in the series of

---

(35) Geisselman, A.; Pilawa, P. Private communication.

(36) Lascialfari, A.; Gatteschi, D.; Borsa, F.; Cornia, A. *Phys. Rev. B* **1997**, *55*, 14341.

(37) Le Gall, F.; Biani, F. F.; Caneschi, A.; Cinelli, P.; Cornia, A.; Fabretti, A. C.; Gatteschi, D. *Inorg. Chim. Acta* **1997**, *262*, 123.

cyclic clusters or is negligibly small compared to $J_{\alpha 1}$. We favor the second interpretation since it sounds more likely that the magnetic orbitals are oriented in a way that the overlap in one direction is very small, rather than that the overlap is independent of the bridge angle.

For the single-ion anisotropy D^{lig} one finds no distinct trend with α, α_2, or α_1. A plot of D^{lig} versus α_1 would essentially reproduce Figure 9 since J and α_1 are linearly correlated. According to Figure 9 it is meaningless to consider L-clusters and L*-clusters simultaneously. In the following we restrict ourselves to the L-clusters.

Since D^{lig} is mainly determined by the coordination geometry of the iron centers, we carefully investigated it for the series of L-clusters. We found that, except for μ_3O_{vic}, the coordination sphere is rather robust. That is, the relative positions of the ions (with regard to the iron center) differ only slightly within the four clusters: The distance of the nitrogen exhibits the largest deviation with 0.10 Å, followed by μ_3O_{ipso} (0.07 Å), for the remaining oxygens the deviation is less than 0.05 Å. The relative donor−Fe−donor angles vary by less than 7°. Exceptions are found only for relative angles involving μ_3O_{vic} Since the angle N−Fe−μ_3O_{vic} (151.2−152.6°) as well as the distance Fe−μ_3O_{vic} (1.978−2.030 Å) remains almost constant, the displacement of μ_3O_{vic} is most easily recognized as a rotation around the N−Fe axis. The rotation angle φ is measured with respect to the plane spanned by the nitrogen, the iron, and μ_1O_{ipso} (inset of Figure 10b). While φ differs by less than 7° for the other oxygens, it changes by as much as 30° for μ_3O_{vic}. This rotation of μ_3O_{vic} is by far the most notable structural variation in the series of the L-clusters, and we thus regard it to be most responsible for the behavior of D^{lig}. Indeed, plotting D^{lig} as function of φ demonstrates a remarkable correlation (Figure 10b). The best-fit straight line is

$$D^{lig}[\mathrm{K}] = 0.0196\,\varphi[°] - 2.65 \qquad (11)$$

It is noteworthy that it is exactly μ_3O_{vic} which is also involved in the Fe−O−Fe bridge arm exhibiting the smaller angle α_1 which controls J. To some extent this explains the approximate correlation of D^{lig} with J visible in Figure 9 for the L-clusters.

Acknowledgment. O.W. and S.S. would like to thank P. van der Linden for his support and kind hospitality during their stay at the GHFML. O.W. also would like to thank W. Biberacher for important information about the M6 magnet environment. Financial support by the Bayerisches Langzeitprogramm “Neue Werkstoffe”, the Deutsche Forschungsgesellschaft, and through the TMR Program of the European Community under contract No. ERBFM-GECT950077 is gratefully acknowledged.

Supporting Information Available: The crystallographic parameters for **2** have been deposited as a CIF file. This material is available free of charge via the Internet at http://pubs.acs.org.

IC0012827